

## RESEARCH ARTICLE

## Generation and Decay Mechanisms of Ningaloo Niño/Niña

10.1002/2017JC012966

Takahito Kataoka<sup>1,2</sup> , Tomoki Tozuka<sup>3</sup> , and Toshio Yamagata<sup>4</sup> 

## Special Section:

Midlatitude Marine Heatwaves: Forcing and Impacts

## Key Points:

- Mechanisms for Ningaloo Niño/Niña are examined by calculating the mixed-layer temperature balance of variable mixed-layer depth
- Sensitivity change in the warming by the climatological solar radiation due to mixed-layer depth anomaly plays a key role in the development
- Latent heat flux as a whole does not directly contribute to anomalous warming/cooling during the development phase

## Supporting Information:

- Supporting Information S1

## Correspondence to:

T. Kataoka,  
tkataoka@15.alumni.u-tokyo.ac.jp

## Citation:

Kataoka, T., Tozuka, T., & Yamagata, T. (2017). Generation and decay mechanisms of Ningaloo Niño/Niña. *Journal of Geophysical Research: Oceans*, 122, 8913–8932. <https://doi.org/10.1002/2017JC012966>

Received 13 MAR 2017

Accepted 20 SEP 2017

Accepted article online 25 OCT 2017

Published online 19 NOV 2017

<sup>1</sup>Atmosphere and Ocean Research Institute, University of Tokyo, Kashiwa, Japan, <sup>2</sup>Now at Project Team for Advanced Climate Modeling, JAMSTEC, Yokohama, Japan, <sup>3</sup>Department of Earth and Planetary Science, Graduate School of Science, University of Tokyo, Tokyo, Japan, <sup>4</sup>Application Laboratory, JAMSTEC, Yokohama, Japan

**Abstract** Using an ocean model, generation and decay mechanisms of warm/cool sea surface temperature anomalies (SSTAs) off Western Australia, or Ningaloo Niño/Niña, are investigated through the calculation of a mixed-layer temperature (MLT) balance taking the mixed-layer depth (MLD) variation into account. Since Ningaloo Niño/Niña develops owing to local air-sea interaction and/or remote forcing, events are classified into two cases based on alongshore wind anomalies and analyzed separately. It is revealed that the anomalous meridional advection associated with the stronger Leeuwin Current and the enhanced warming by the climatological shortwave radiation because of the shallower MLD generate warm SSTAs in the coastal region for both cases of Ningaloo Niño. On the other hand, the latent heat flux damps SSTAs only in a case without northerly alongshore wind anomalies. In the decay, larger sensible heat loss is important. Because of the reduced meridional temperature gradient, the meridional advection eventually damps SSTAs. The sensitivity change to the climatological shortwave radiation owing to MLD anomalies explains offshore MLT tendency anomalies for both cases throughout the events. The mechanisms for Ningaloo Niña are close to a mirror image of Ningaloo Niño but differ in that the latent heat flux damps offshore SSTAs. The seasonal phase-locking nature of Ningaloo Niño/Niña is related to the seasonal variations of MLD and surface heat fluxes, which regulate the amplitude and sign of the sensitivity change to surface heat fluxes. It is also related to the seasonal variations of the Leeuwin Current and meridional temperature gradient through advection anomalies.

## 1. Introduction

The dominant interannual variation of sea surface temperature (SST) in the southeastern Indian Ocean along the west coast of Australia is characterized by an El Niño/La Niña-like warming/cooling and is called Ningaloo Niño/Niña (Feng et al., 2013; Kataoka et al., 2014; Figure 1a). Typically, it develops during austral spring (hereafter, seasons refer to those for the Southern Hemisphere), peaks during summer, and decays in the following autumn (Kataoka et al., 2014; Figure 1c). The 2010/2011 Ningaloo Niño was the strongest event ever recorded instrumentally and caused a devastating coral bleaching event (Pearce & Feng, 2013) and changes in the marine ecosystem (Wernberg et al., 2012). Also, it is shown that northwestern Australia tends to receive more/less rainfall during Ningaloo Niño/Niña (Tozuka et al., 2014). Therefore, understanding mechanisms of Ningaloo Niño/Niña is important.

Using observational data sets, Kataoka et al. (2014) have examined the mechanism of Ningaloo Niño/Niña during the past 60 years and classified the events into the locally and nonlocally amplified cases based on the local alongshore wind anomalies in summer. The former case develops mostly through an intrinsic air-sea interaction: An anomalous low/high generated by positive/negative SST anomalies (Tozuka et al., 2014) is accompanied by northerly/southerly alongshore wind anomalies, which cause coastal downwelling/upwelling anomalies as well as stronger/weaker poleward-flowing Leeuwin Current and further enhance the initial SST anomalies. On the other hand, in the latter case, negative/positive sea level pressure (SLP) anomalies over the Australian continent for Ningaloo Niño/Niña, result in a band-like pattern of SLP anomalies with no anomalous alongshore wind. As a consequence, the relative importance of the intrusion of the oceanic downwelling/upwelling coastal waves that cause positive/negative SST anomalies through the strengthened/weakened Leeuwin Current becomes larger. These waves originate from the western Pacific and/or northern coast of Australia, with the former related to the El Niño/Southern Oscillation (ENSO; Clarke, 1991; Clarke & Liu, 1994; Meyers, 1996). We note that the ENSO also generates SLP anomalies off Western

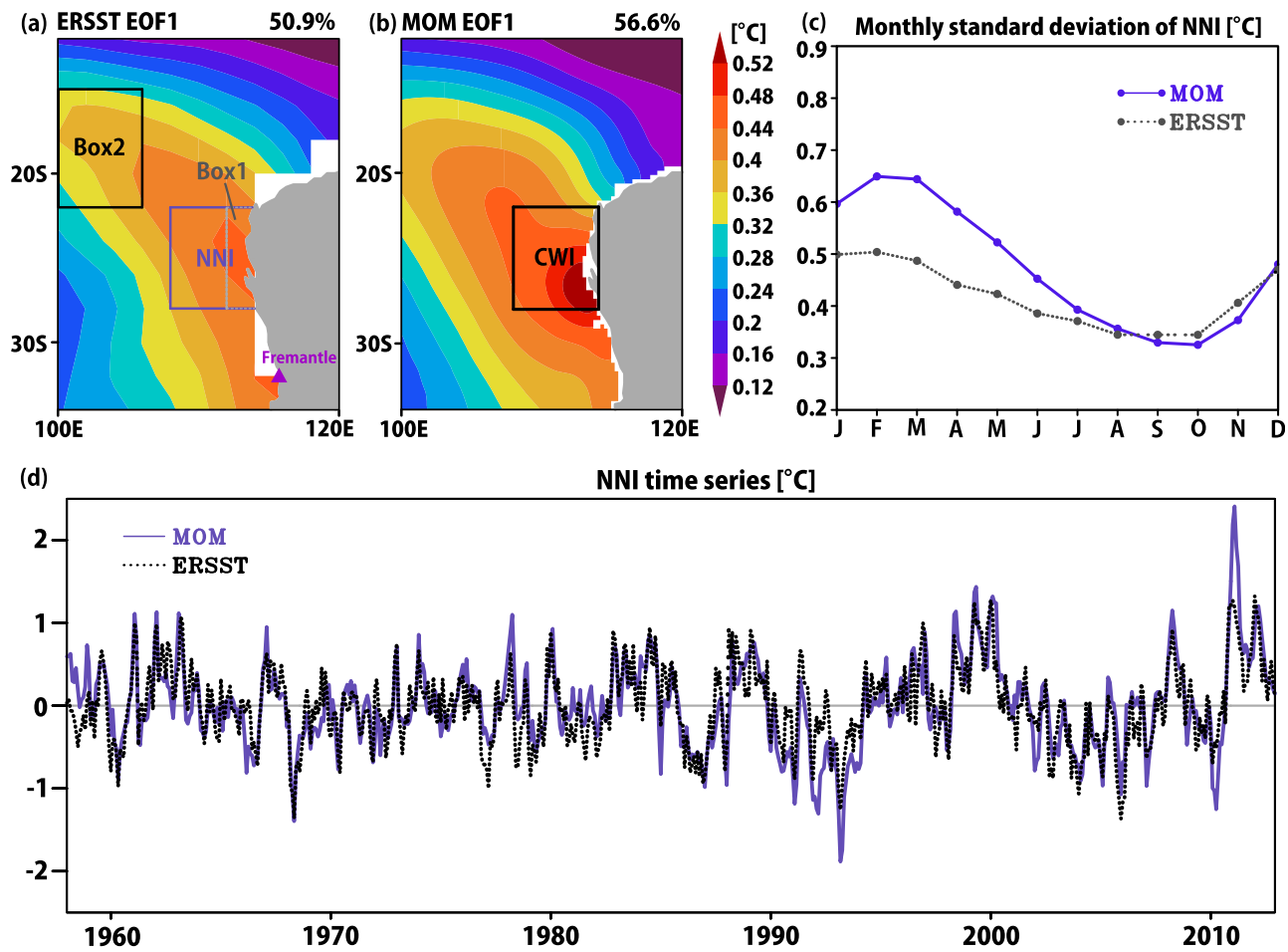


**Figure 1.** First empirical orthogonal function (EOF) mode of sea surface temperature (SST) anomalies off Western Australia for (a) ERSST and (b) the model. Variance contribution is indicated on the top right of each figure. In Figure 1a, the domain used to calculate the Ningaloo Niño index (NNI; 108°E-coast, 28°S–22°S; blue solid) and mixed-layer temperature (MLT) balance for the coastal region (Box 1: 112°E-coast, 28°S–22°S; gray dotted) and the offshore region (Box 2: 100–106°E, 22–15°S; black solid) are indicated, whereas the domain used to define the coastal wind index (CWI; 108–114°E, 28–22°S; black solid) is superimposed in Figure 1b. The location of Fremantle is also indicated in Figure 1a by a triangle. (c) Monthly standard deviation of the 3 month running averaged NNI (blue solid: the model, gray dotted: ERSST). (d) Time series of simulated (blue solid) and observed (black dotted) NNI.

Australia and influences the local alongshore wind anomalies. Therefore, this remote atmospheric effect may influence the locally amplified case, but the classification by Kataoka et al. (2014) is simply based on whether local wind anomalies contribute to a local amplification of SST anomalies. In addition, Kataoka et al. (2014) have suggested that latent heat flux anomalies may contribute to the further growth of SST anomalies in the coastal region at the peak phase and to SST anomaly generation in the offshore region during the development. Their analysis regarding the surface heat fluxes, however, was based on the composite spatial patterns and thus, they did not incorporate the effects of interannual variations in mixed-layer depth (MLD) on the surface heat fluxes.

Also, the above studies did not discuss the mechanism quantitatively. In this regard, Benthuisen et al. (2014) were the first to conduct the heat budget analysis using a regional ocean model. They showed that the anomalously strong Leeuwin Current and surface heat flux anomalies play an important role in the anomalous warming in the 2010/2011 event, supporting the earlier work by Feng et al. (2013).

More recently, Marshall et al. (2015) have examined the heat budget of the upper 50 m during the warming events of the past 50 years using reanalysis data sets. They have shown that latent heat flux anomalies, together with the anomalous advection by the Leeuwin Current, directly generated positive SST anomalies. These studies, however, have conducted the heat budget analysis by assuming the ocean mixed-layer thickness to be constant. This assumption needs to be scrutinized considering that the MLD undergoes

significant seasonal and interannual variations and the sensitivity of the mixed-layer to surface heat fluxes is dependent on the MLD. In addition, Marshall et al. (2015) have not introduced any distinction between the locally and nonlocally amplified events despite that Kataoka et al. (2014) demonstrated that two different mechanisms (i.e., the local ocean-atmosphere coupled process and the remote forcing) are important.

The above has motivated us to investigate how local ocean temperature anomalies of locally and nonlocally amplified Ningaloo Niño/Niña are generated and damped using an ocean general circulation model (OGCM). In particular, we focus on possible influences of the MLD variation. The key questions to be addressed are: Are there any differences in the processes involved in the evolution of the locally and nonlocally amplified cases? Do variations in the MLD play any role? If so, what process is more responsible for the SST warming or cooling?

The rest of this paper is organized as follows. A brief description of observational and reanalysis data sets and model simulations is given in the next section. Section 3 describes and develops a diagnostic method for examining a mixed-layer temperature (MLT) balance; a more detailed derivation for some equations is presented in the supporting information. The seasonal variation is examined in section 4 and main results for interannual variations are presented in section 5. Discussions and conclusions are given in sections 6 and 7, respectively.

## 2. Model and Data

The OGCM used in this study is based on version 3.0 of the Modular Ocean Model (MOM3.0; Pacanowski & Griffies, 1999) developed at the National Oceanic and Atmospheric Administration/Geophysical Fluid Dynamics Laboratory (NOAA/GFDL). The model covers the global ocean for 65°S–65°N, where the horizontal resolution varies from 1/4° around the study region (90°E–160°E, 40°S–20°N) to 2° (1°) in the zonal (meridional) direction in the outer region. The region with the finest resolution encompasses the Ningaloo Niño/Niña-related SST anomalies (Feng et al., 2013; Kataoka et al., 2014; Marshall et al., 2015). Within the sponge layer of 3° latitudinal width from the model northern and southern boundaries, temperature and salinity are strongly restored toward the monthly climatology (Levitus & Boyer, 1994; Levitus et al., 1994) to reduce artificial wall effects. There are 25 vertical levels and the 5 min gridded elevation data from ETOPO5 are adopted for the bottom topography and the coastlines. The lateral eddy viscosity and diffusivity are based on the formula given by Smagorinsky (1963) and the parameterization of Pacanowski and Philander (1981) is used for the vertical eddy viscosity and diffusivity calculation.

The model is first spun up for 20 years from the initial state of no motion with the annual mean climatology (Levitus & Boyer, 1994; Levitus et al., 1994) by the monthly climatology of the wind stress from the National Centers for Environmental Prediction/National Center for Atmospheric Research (NCEP/NCAR) reanalysis data (Kalnay et al., 1996) and the surface heat flux calculated by the bulk formulae using simulated SSTs and the atmospheric variables from the reanalysis. Simulated sea surface salinities (SSSs) are relaxed to the monthly mean climatology with the restoring time scale of 30 days. Then, it is further integrated using the daily mean wind stress from the NCEP/NCAR reanalysis and daily surface heat flux calculated by the bulk formulae for 1948–2012 with the spin-up period of the first 10 years discarded. Thus, outputs for the last 55 years from 1958 to 2012 are analyzed. Again, simulated SSSs are nudged toward the monthly mean climatology.

For comparison, we use the Extended Reconstructed Sea Surface Temperature (ERSST) version 3b data set (Smith et al., 2008) with 2° × 2° resolution from 1958 to 2012. Ocean currents from the Simple Ocean Data Assimilation (SODA; Carton & Giese, 2008) for 1958–2010 and from the Predictive Ocean Atmosphere Model for Australia Ensemble Ocean Data Assimilation System Re-Analysis (PEODAS; Yin et al., 2011) for 1981–2010 are adopted. The sea level observations at Fremantle (115°44'E, 32°03'S; Figure 1a) are obtained from the National Tidal Unit (NTU). Monthly climatology of MLD from Commonwealth Scientific and Industrial Research Organisation (CSIRO) Atlas of Regional Seas 2009 (CARS2009; Ridgway et al., 2002) is used as well, where MLD is defined as a smaller depth at which the temperature decreases by 0.2°C or the salinity increases by 0.03 practical salinity unit from 10 m. For MLD diagnosis, monthly climatology of evaporation minus precipitation from the European Centre for Medium-Range Weather Forecasts Interim Reanalysis (ERA-Interim; Dee et al., 2011) for the period 1979–2014 is used.

Linear trends are removed from the observation data and outputs from the OGCM using a least squares fit. When discussing the MLD and MLT balance, however, we retain trends to avoid artificial inversion layers.

### 3. Mixed-Layer Temperature Balance: Physical Background

The MLT balance can be calculated by

$$\frac{\partial T_{\text{mix}}}{\partial t} = \frac{Q}{\rho c_p h} - \frac{1}{h} \int_{-h}^0 \mathbf{v} \cdot \nabla_h T dz - \frac{1}{h} \int_{-h}^0 \nabla_h \cdot (\kappa_h \nabla_h T) dz + \frac{q_{-h}}{\rho c_p h} \quad (1)$$

(e.g., Vialard & Delecluse, 1998). Here  $T_{\text{mix}}$  is temperature averaged over the mixed-layer,  $\rho$  is the sea water density,  $c_p$  is the specific heat of the sea water,  $h$  is the MLD, which is defined as a depth at which the potential density increases by  $0.01 \text{ kg/m}^3$  from the top model level,  $\mathbf{v}$  is horizontal velocity vector,  $T$  is the sea water temperature,  $\kappa_h$  is the horizontal diffusion coefficient,  $q_{-h}$  is the heat flux at the bottom of the mixed-layer representing vertical diffusion, entrainment, and vertical advection, and  $\nabla_h$  is a horizontal gradient operator. Also, the net surface heat flux  $Q$  is given by

$$\begin{aligned} Q &= Q_{\text{sw}} + Q_{\text{lw}} + Q_{\text{lh}} + Q_{\text{sh}} \\ &= q(0) - q(-h) + Q_{\text{lw}} + Q_{\text{lh}} + Q_{\text{sh}}, \end{aligned} \quad (2)$$

where  $Q_{\text{sw}}$  is the shortwave radiation absorbed in the mixed-layer, and  $Q_{\text{lw}}$ ,  $Q_{\text{lh}}$ , and  $Q_{\text{sh}}$  are the net surface longwave radiation, latent heat flux, and sensible heat flux, respectively. Also,  $q(z)$  is the downward shortwave radiation at depth  $z$  and is parameterized by

$$q(z) = q(0) \left[ R \exp\left(-\frac{z}{\gamma_1}\right) + (1-R) \exp\left(-\frac{z}{\gamma_2}\right) \right] \quad (3)$$

(Paulson & Simpson, 1977), where  $R (=0.58)$  is a separation constant, and  $\gamma_1$  ( $0.35 \text{ m}$ ) and  $\gamma_2$  ( $=23.0 \text{ m}$ ) are attenuation length scales. These values are for the case of water type I of Jerlov (1976). For the rest of the paper, we denote the surface heat flux into the ocean as positive heat flux.

The modeled longwave radiation into the ocean is calculated using the observed and modeled SSTs (in  $^{\circ}\text{C}$ ; denoted by  $SST^{\text{obs}}$  and  $SST$ , respectively) and the longwave radiation from the reanalysis ( $Q_{\text{lw}}^{\text{obs}}$ ) as follows:

$$Q_{\text{lw}} = Q_{\text{lw}}^{\text{obs}} + e_m \sigma \left[ (SST^{\text{obs}} + 273.16)^4 - (SST + 273.16)^4 \right], \quad (4)$$

where  $e_m = 0.97$  is the seawater emissivity and  $\sigma = 5.67 \times 10^{-8} \text{ W m}^{-2} \text{ K}^{-4}$  is the Stefan-Boltzmann constant.

The latent and sensible heat fluxes are computed using bulk formulae:

$$Q_{\text{lh}} = -\rho_a L C_E \Delta q WS, \quad (5)$$

$$Q_{\text{sh}} = -\rho_a C_{pa} C_H (SST - T_2) WS. \quad (6)$$

Here  $\rho_a = 1.2 \text{ kg m}^{-3}$  is the air density,  $L = 2.5 \times 10^6 \text{ J kg}^{-1}$  the latent heat of vaporization,  $C_E = C_H = 1.5 \times 10^{-3}$  the bulk transfer coefficients,  $WS$  the wind speed at  $10 \text{ m}$ ,  $C_{pa} = 1.005 \times 10^3 \text{ J kg}^{-1}$  the specific heat of the air,  $T_2$  the air temperature at  $2 \text{ m}$ , and  $\Delta q \equiv q_s - q_a$  the difference between the saturated specific humidity at the sea surface ( $q_s$ ) and the specific humidity at  $2 \text{ m}$  ( $q_a$ ). Letting  $e_s = 6.1121 \exp \left[ \frac{18.729 - SST}{227.3} \right] \frac{SST}{SST + 257.87}$  be the saturated vapor pressure in hPa and  $P_s = 1013.0 \text{ hPa}$  be the sea level pressure,  $q_s$  is obtained by

$$q_s = 0.62197 e_s / (P_s - 0.378 e_s).$$

Although the first term on the RHS of equation (1) represents the contribution from the surface heat flux, it should not be treated as a simple quantity because its variation is a combination of the effects of changes in the surface heat fluxes and MLD. As noted in the introduction, the latter effect could modulate the former, but it was not considered in the previous studies. Hence, decomposition into one from actual surface heat flux variability and another from MLD variations helps us to understand their relative importance in the evolution of Ningaloo Niño/Niña. A Taylor expansion for the first term on the RHS of equation (1) about the monthly climatology gives

$$\left(\frac{Q}{\rho c_p \bar{h}}\right)' = \frac{Q'}{\rho c_p \bar{h}} - \frac{\bar{Q}}{\rho c_p \bar{h}} \frac{h'}{\bar{h}} + \text{Res.} \quad (7)$$

Here an overbar (a prime) denotes monthly climatology (interannual anomaly) and we have assumed  $|Q'/\bar{Q}| \ll 1$  and  $|h'/\bar{h}| \ll 1$ . For a more detailed derivation, readers may refer to the supporting information. The first term on the RHS represents an anomalous contribution from the surface heat flux anomaly and is referred to as “heat flux anomaly effect” for convenience. The second term on the RHS shows the variation in sensitivity to the climatological surface heat flux associated with the variation in heat capacity of the mixed-layer associated with MLD anomaly and called “heat capacity variation effect” in this paper. For example, when the mixed-layer is anomalously deep (positive  $h'$ ), the climatological cooling by the latent heat flux weakens due to the larger mixed-layer heat capacity, resulting in warm MLT anomalies if everything else remains the same. Equation (7) is also applicable to anomalous contribution from the vertical heat flux at the bottom of the mixed-layer, that is, the last term on the RHS of equation (1) ( $Q$  is replaced with  $q_{-h}$ ).

Since our focus is on summer, when the mixed-layer is shallow, we note that even when the incoming shortwave radiation at the sea surface remains the same, the shortwave radiation anomaly,  $Q'_{sw}$ , may include nonnegligible contribution from the anomalous penetrative shortwave radiation at the base of the mixed-layer associated with MLD anomalies. Therefore, it would be helpful to separate it from the contribution from a surface shortwave radiation anomaly on the interannual timescale. Since  $O(R) \sim O(1-R)$  and  $O(h) \sim O(\gamma_2) \gg O(\gamma_1)$ , only the second term on the RHS of equation (3) is influential at the base of a mixed-layer, giving

$$Q_{sw} = q(0) \left[ 1 - \left( R \exp\left(-\frac{h}{\gamma_1}\right) + (1-R) \exp\left(-\frac{h}{\gamma_2}\right) \right) \right] \approx q(0) \left[ 1 - (1-R) \exp\left(-\frac{h}{\gamma_2}\right) \right]. \quad (8)$$

Using a Taylor expansion and supposing that  $|q(0)'/q(0)| \ll 1$  and  $|h'/\gamma_2| \ll 1$ , an anomaly in the shortwave radiation absorbed in a mixed-layer is represented by

$$Q'_{sw} \approx q(0)' \left[ 1 - (1-R) \exp\left(-\frac{\bar{h}}{\gamma_2}\right) \right] + \left[ \frac{q(0)}{q(0)} (1-R) \exp\left(-\frac{\bar{h}}{\gamma_2}\right) \right] \frac{h'}{\gamma_2} + \text{Res.} \quad (9)$$

Thus, the decomposition of the contribution from the shortwave radiation may be written as

$$\left(\frac{Q_{sw}}{\rho c_p \bar{h}}\right)' \approx \frac{q(0)'}{\rho c_p \bar{h}} \left[ 1 - (1-R) \exp\left(-\frac{\bar{h}}{\gamma_2}\right) \right] + \frac{\left[ \frac{q(0)}{q(0)} (1-R) \exp\left(-\frac{\bar{h}}{\gamma_2}\right) \right] \frac{h'}{\gamma_2}}{\rho c_p \bar{h}} - \frac{\bar{Q}_{sw}}{\rho c_p \bar{h}} \frac{h'}{\bar{h}} + \text{Res.} \quad (10)$$

Here the first term on the RHS is the contribution from the shortwave radiation anomaly at the sea surface, and the second term represents the effect of variation in absorption amount due to the MLD anomaly (“absorption anomaly effect”). The third term is the contribution from the heat capacity variation for the shortwave radiation.

The second term on the RHS of equation (1), which denotes the horizontal advection, is also influenced by several factors (i.e., interannual variations in the MLD, ocean currents, and horizontal temperature gradient). Thus, a diagnostic equation to examine the relative importance of the above factors is useful. Assuming that  $|h'/\bar{h}| \ll 1$ ,  $|v'/\bar{v}| \ll 1$ , and  $|\nabla_h T'/\nabla_h \bar{T}| \ll 1$ , the horizontal advection anomaly term may be decomposed as

$$\left(-\frac{1}{h} \int_{-h}^0 \mathbf{v} \cdot \nabla_h T dz\right)' = - \left[ (\bar{\mathbf{v}} \cdot \nabla_h \bar{T})|_{-\bar{h}} - \frac{1}{\bar{h}} \int_{-\bar{h}}^0 \bar{\mathbf{v}} \cdot \nabla_h \bar{T} dz \right] \frac{h'}{\bar{h}} - \frac{1}{\bar{h}} \int_{-\bar{h}}^0 \mathbf{v}' \cdot \nabla_h \bar{T} dz - \frac{1}{\bar{h}} \int_{-\bar{h}}^0 \bar{\mathbf{v}} \cdot \nabla_h T' dz + \text{Res.} \quad (11)$$

Here a Taylor expansion is used again. We note that a variational method with an additional assumption leads to the same result (see the supporting information for more detail). The sum of the first two terms

represents the effect of the vertical shear in climatological horizontal advection (“shear effect”). The third is associated with the anomalous advection of the mean temperature gradient. In a similar manner, the fourth term is related to the mean advection of the anomalous horizontal temperature gradient.

Considering that the third term on the RHS of equation (1), which represents the horizontal diffusion, is expected to be small, we may estimate the fourth term, which we refer to as a vertical term or vertical processes, by taking the difference between the LHS and the first two terms on the RHS.

Since we expect SST anomalies in the coastal and offshore regions may be generated by different mechanisms due to different roles of the Leeuwin Current and coastal processes (e.g., Marshall et al., 2015), we calculate the MLT balance in two box regions (Figure 1a). Box 1 (112°E-coast, 28°S–22°S) is located within the Ningaloo Niño/Niña index (NNI) region (108°E-coast, 28°S–22°S), whereas Box 2 (100°E–106°E, 22°S–15°S) is located away from the coast. The NNI is defined as SST anomalies averaged over the region 108°E-coast, 28°S–22°S, where the highest SST variability of Ningaloo Niño/Niña occurs (Figure 1a). Anomalies are computed with respect to the monthly mean climatology of 1958–2012.

#### 4. Seasonal Cycles

Prior to examining the MLT balance during Ningaloo Niño/Niña years, we analyze the seasonal cycle of the study region. Both observed and simulated SSTs in Boxes 1 and 2 reach the maximum in late summer to early autumn and the minimum around spring (Figure 2a). Also, the MLD in these regions shoals in summer and deepens in fall and winter (Figure 2b). To obtain an insight into the seasonal variation of the MLD, the simulated MLD is recalculated with temperature and/or salinity replaced by their annual mean climatology:  $h(\overline{T^a}, \overline{S^a})$ ,  $h(\overline{T^a}, S)$  and  $h(T, \overline{S^a})$  (an overbar with superscript *a* denotes the annual mean climatology; Figures 2c and 2d). It is found that simulated MLDs in both regions are mainly determined by temperature profiles rather than salinity profiles since  $h(T, \overline{S^a})$  relative to  $h(\overline{T^a}, \overline{S^a})$  reproduces the seasonal cycle better than  $h(\overline{T^a}, S)$  relative to  $h(\overline{T^a}, \overline{S^a})$ , though we note that SSSs are restored to the observed monthly climatology in our model. The model overestimates the MLD in winter and this may be partly due to the lack of the diurnal cycle. While the daily mean surface heat flux is negative in winter, the surface heating during the daytime stabilizes the upper layer (e.g., Ide & Yoshikawa, 2016). Hence, including the diurnal cycle in the surface boundary condition may reduce this bias. However, the MLD in summer when Ningaloo Niño/Niña develops is realistically simulated. We leave details of the MLD bias in winter for future study.

The warming (cooling) tendency of the mixed-layer over both regions in summer (winter) is consistent with the seasonal cycle of SSTs (Figures 2e and 2f). While these tendencies are mostly explained by the contribution from the surface heat flux, whose seasonal variation is dominated by the shortwave radiation (figure not shown), the meridional advection modulates the seasonal variation in the coastal region during late summer to autumn because of the seasonal strengthening of the Leeuwin Current (Figure 3). In addition, the seasonal intensification of the meridional temperature gradient in summer may contribute to the stronger meridional advection. The seasonal strengthening of the Leeuwin Current seems to be due to slackening of southerly winds (Godfrey & Ridgway, 1985; Smith et al., 1991) or to the pressure rise to the north (Godfrey & Ridgway, 1985). The reproduced seasonality of the current is consistent with the data assimilation products (Figure 3) and is also verified by the high correlation coefficient of 0.92 between the simulated and observed climatology of sea level at Fremantle, which is considered to be a good proxy for the Leeuwin Current strength (Feng et al., 2003). Vertical processes contribute to the cooling during summer. Since the mixed-layer shoals, the entrainment is expected to be small. Rather, a more efficient cooling of the seasonally thin mixed-layer by vertical diffusion may explain this cooling.

#### 5. Interannual Variations: Ningaloo Niño/Niña

We begin by performing an empirical orthogonal function (EOF) analysis on SST anomalies to extract the dominant mode of interannual variability off the west coast of Australia (100°E–120°E, 34°S–12°S; Figures 1a and 1b). The model well reproduces the observed spatial pattern and amplitude of Ningaloo Niño/Niña with a pattern correlation coefficient of 0.94, which is better than the state-of-the-art coupled models (Kido et al., 2016); we note that our simulation has an advantage of having reanalysis data as the surface boundary conditions. The current model well simulates the observed NNI during 1958–2012 (Figure 1d) with a

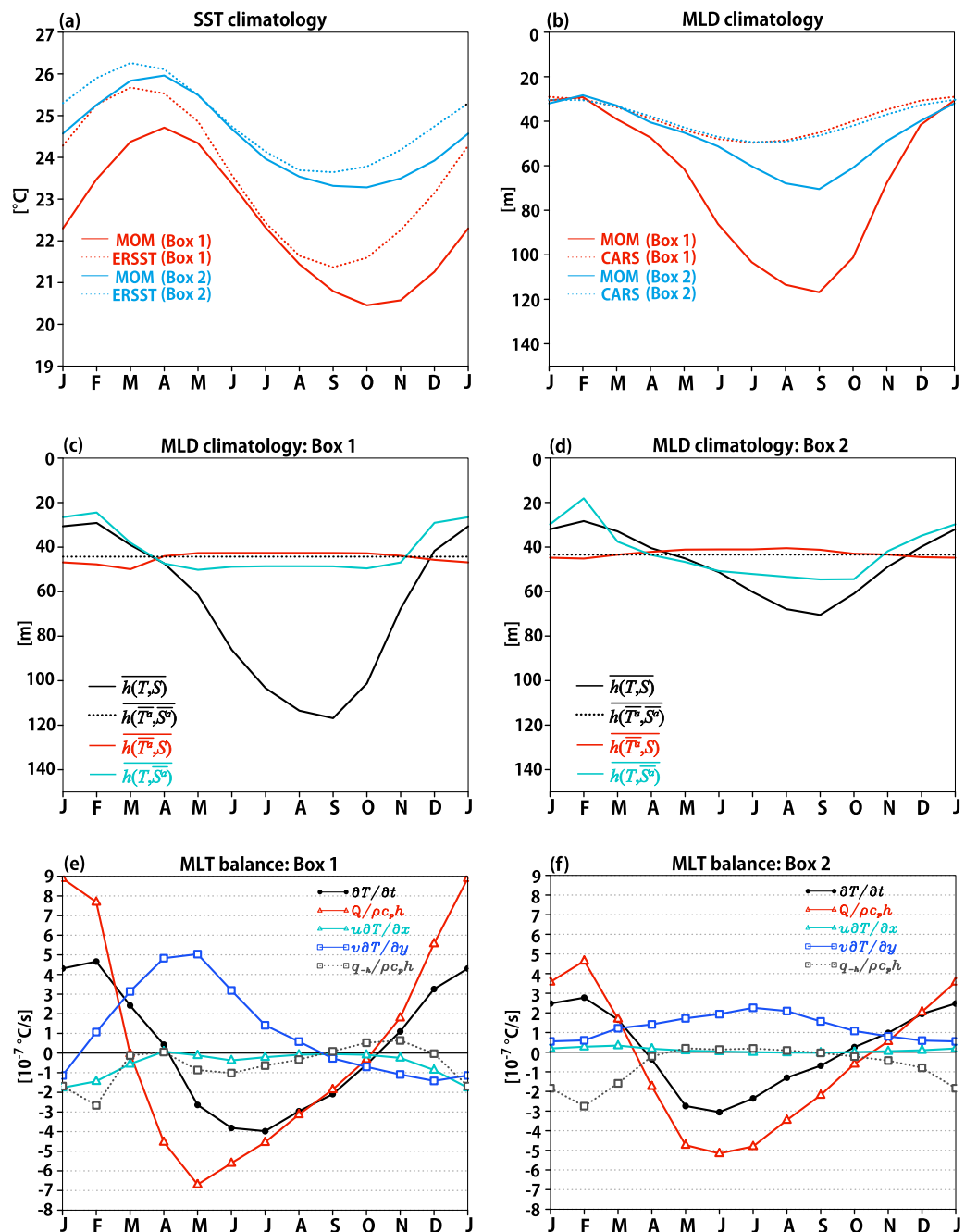


**Figure 2.** (a) Annual cycle of SST from the model (solid line) and the observation (dotted line) for the Box 1 (red) and Box 2 (blue) regions. (b) As in Figure 2a, but for mixed-layer depth (MLD). (c, d) Simulated MLD climatology computed using interannually varying temperature and salinity (black solid), annual mean temperature and salinity (dotted black), annual mean temperature and interannually varying salinity (red), and interannually varying temperature and annual mean salinity (light blue) for the Box 1 and 2 regions. (e) Climatological MLT balance over the Box 1 region. The MLT tendency, the contribution from the surface heat flux, zonal advection, meridional advection, and vertical processes are shown in black, red, light blue, blue, and dotted gray lines, respectively. (f) As in Figure 2e, but for the Box 2 region.

correlation coefficient of 0.81. This is partly because of its success in simulating the Leeuwin Current variability; high correlation of 0.81 is found between observed and simulated sea level anomalies at Fremantle.

The standard deviation of 3 month running averaged NNI is computed to check its seasonality. Both observed and simulated NNI show high (low) variability in summer (winter), although the simulated

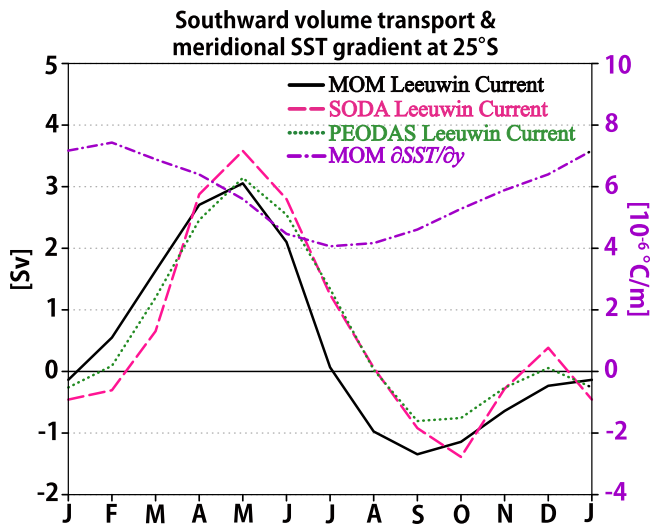


**Figure 3.** Southward volume transport (in Sv) across 108°E-coast at 25°S in the upper 300 m from the model (solid black), SODA (dashed pink), and PEODAS (dotted green). Note that positive values indicate the southward transport. Superimposed is meridional SST gradient (in  $10^{-6}\text{C/m}$ ) across 112°E-coast at 25°S from the simulation (purple dot dash).

amplitude is somewhat stronger in the peak season (Figure 1c). Because of this phase-locking nature, we have decided to define Ningaloo Niño (Niña) years as the years in which the simulated NNI averaged over January–March is above 1 (below  $-1$ ) standard deviation with year 0 regarded as the Ningaloo Niño/Niña-developing year and year 1 as the following year. This criterion leads to 13 (11) Ningaloo Niño (Niña) years (Figure 4), where the years in black letters are the same as those defined by Kataoka et al. (2014) using the ERSST data. The current model reproduces most events but fails to capture the 1982/1983 and 1996/1997 Ningaloo Niño and the 1976/1977 Ningaloo Niña events in Kataoka et al. (2014). We note that these are “borderline events” and the model simulates moderate events just below the criteria (Figure 1d). To classify the simulated events into two cases following Kataoka et al. (2014), we calculate the coastal wind index (CWI), which is defined by the area-average of northerly wind anomalies over the coastal region (108°E–114°E, 28°S–22°S; Figure 1b), as shown in Figure 4. Ningaloo Niño (Niña) events with the CWI exceeding 0.9 (below  $-0.9$ ) standard deviations are classified as “locally amplified case,” whereas the others are classified as “nonlocally amplified case” (see Figure 4 for event years). The composites are computed by averaging monthly anomaly fields for each of the four cases defined above (six events for the locally amplified Ningaloo Niño, seven events for the nonlocally amplified Ningaloo Niño, three events for the locally amplified Ningaloo Niña, and eight events for the nonlocally amplified Ningaloo Niña). Unless otherwise noted, qualitatively the same results are obtained even when only the sign of the CWI is used for the criterion.

### 5.1. Ningaloo Niño

#### 5.1.1. Locally Amplified Case

##### 5.1.1.1. Coastal Region

Figure 5a shows the composite of MLT balance in Box 1 for the locally amplified case. The significant warming in summer is primarily driven by two major contributions from the anomalous meridional advection and shortwave radiation. The former is mostly explained by anomalous strengthening of the Leeuwin Current (Figure 6a blue line; the third term on the RHS of equation (11) with  $v' < 0$ ). This supports the hypothesis of the local feedback process proposed by Kataoka et al. (2014) based on the observation, in which alongshore northerly wind anomalies accelerate the Leeuwin Current. This is also consistent with their viewpoint based on energetics; a positive correlation between atmospheric surface wind anomalies and

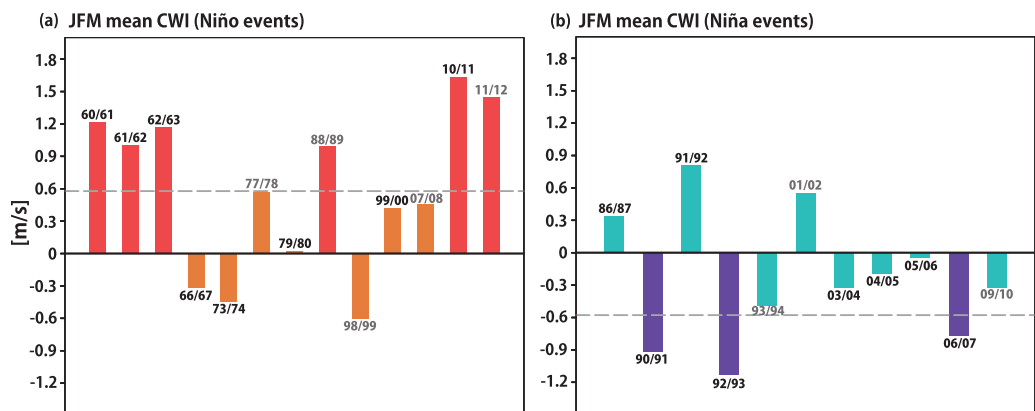


**Figure 4.** (a) January–March (JFM) mean CWI in each Ningaloo Niño year. The dashed line represents 0.9 standard deviation of the CWI. The “locally amplified cases” are drawn in red, whereas the “nonlocally amplified cases” are in orange. Years in black letters are the same as those identified by Kataoka et al. (2014). (b) As in Figure 4a, but for each Ningaloo Niña year. The dashed line indicates  $-0.9$  standard deviation of the CWI. The “locally amplified cases” are expressed in purple, whereas the “nonlocally amplified cases” are in light blue.

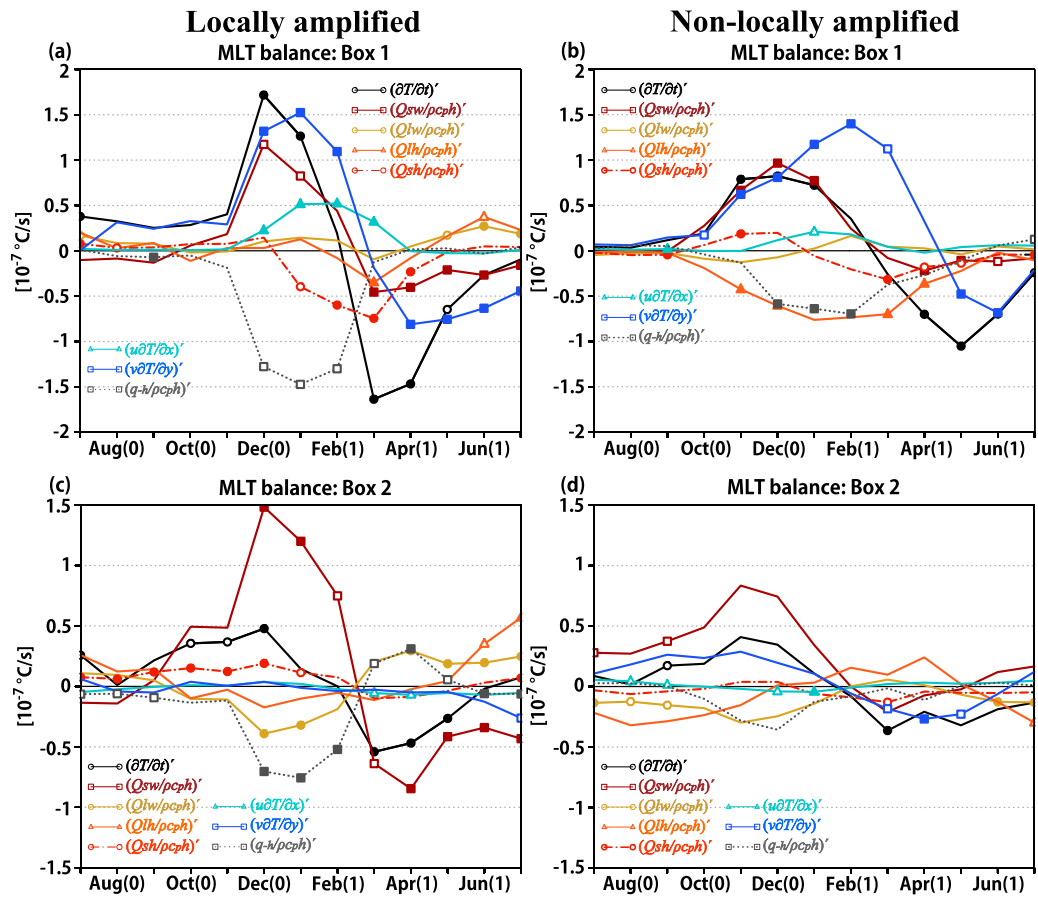


**Figure 5.** Composites of the MLT balance (in  $10^{-7} \text{C/s}$ ) over the Box 1 region in the (a) locally amplified and (b) nonlocally amplified Ningaloo Niño years. The MLT tendency anomaly (black solid line), the anomalous contribution from the short-wave radiation (dark-red solid line), the longwave radiation (yellow solid line), the latent heat flux (orange solid line), and the sensible heat flux (red dot-dash line), the zonal advection anomaly (light-blue solid line), the meridional advection anomaly (blue solid line), and the anomaly in the vertical processes (dark-gray dotted line) are shown. Anomalies exceeding the 90% (80%) confidence level by a two-tailed  $t$  test are indicated by filled (open) markers. A 3 month running mean is applied to smooth the time series. (c, d) As in Figures 5a and 5b, but for the Box 2 region. Note that the different vertical scales are used for Box 1 and Box 2 and that  $10^{-7} \text{C/s} \sim 0.26 \text{C/month}$ .

anomalous oceanic flows in the ML is necessary for instability (see their Appendix). The anomalous meridional advection is further enhanced by seasonal strengthening of the meridional temperature gradient in summer (Figure 3; a larger  $|\nabla \bar{T}|$  in the third term on the RHS of equation (11)) and this may partly explain the seasonality of the phenomenon. The latter contribution from the shortwave radiation also contributes to the warming tendency, offering another possible positive feedback process. This is dominated by the third term on the RHS of equation (10) denoting the heat capacity variation effect due to MLD anomalies (Figure 7a). On the other hand, the heat flux at the bottom of the mixed-layer anomalously cools the mixed-layer as seen in Figure 5a. To obtain further insight into this effect, we calculate the temperature difference ( $\Delta T \equiv T_{\text{mix}} - T_{-10}$ ) between the MLT and the temperature at 10 m below the base of the mixed-layer ( $T_{-10}$ ). We find significant positive  $\Delta T$  anomalies in January (1) and February (1) (not shown), leading to stronger cooling by the vertical entrainment and diffusion. The larger  $\Delta T$  is the result of the warmed mixed-layer at the peak phase. Since MLD anomalies are negative (Figure 7a), the cooling by such vertical processes is amplified as well (the second term on the RHS of equation (7) is negative with  $\bar{q}_{-h} < 0$  and  $h' < 0$ ).

It is interesting to note that no significant contribution from the latent heat flux is seen during the developing seasons, even though previous studies suggested that latent heat flux anomalies contribute to the SST anomaly growth around the peak phase (e.g., Kataoka et al., 2014; Marshall et al., 2015). This apparent contradiction in the coastal region may be explained by a balance between the flux anomaly effect and the

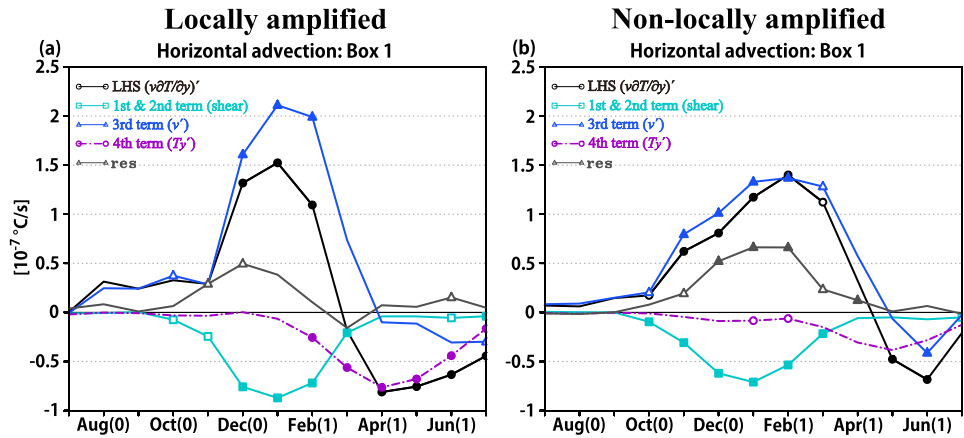


**Figure 6.** Time series of composite anomalies of the meridional advection terms in equation (11) over the Box 1 region for (a) the locally amplified and (b) nonlocally amplified Ningaloo Niño (in  $10^{-7} \text{C/s}$ ). The meridional advection anomaly (black solid line), the sum of the first two terms (light-blue solid line; climatological advection shear effect), the third term (blue solid line; anomalous ocean current effect), the fourth term (purple dot-dash line; meridional temperature gradient anomaly effect), and residual (dark-gray solid line) are shown. Filled (open) markers show anomalies exceeding the 90% (80%) confidence level by a two-tailed  $t$  test. A 3 month running mean is applied to smooth the time series.

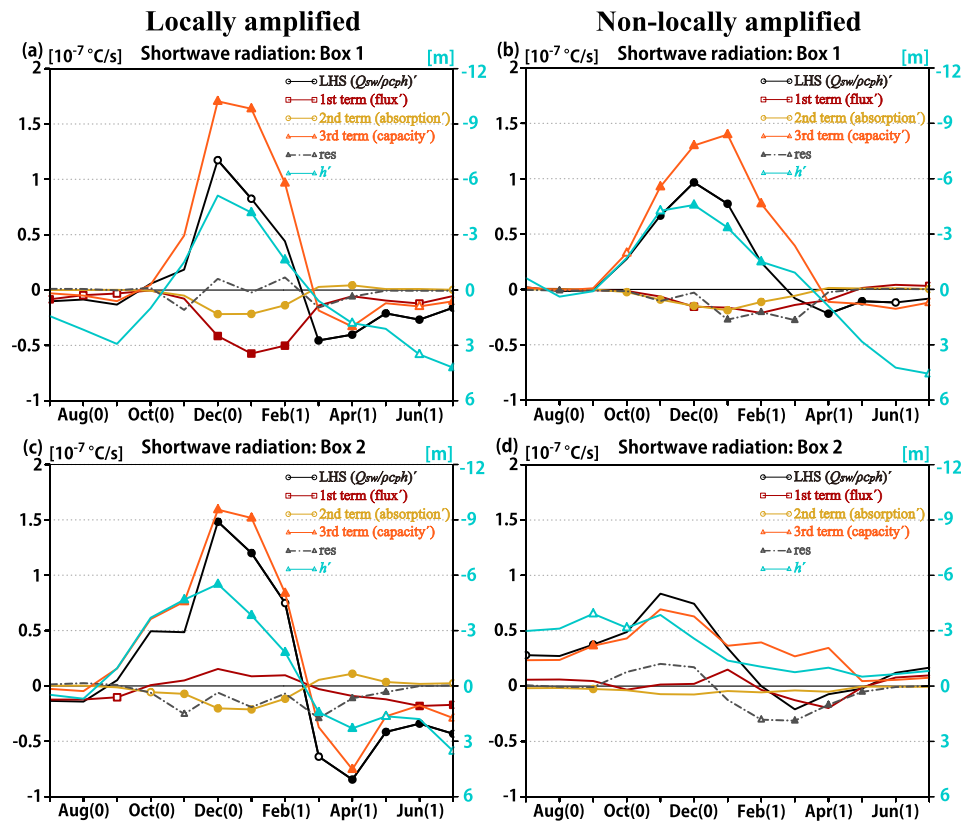


**Figure 7.** Time series of composite anomalies of the shortwave radiation terms in equation (10) for the locally amplified Ningaloo Niño over (a) the Box 1 and (c) Box 2 regions (in  $10^{-7} \text{C/s}$ ; left y axis label). The total contribution anomaly (black solid line), the first term (dark-red solid line; flux anomaly effect), the second term (yellow solid line; variation in absorption amount effect), the third term (orange solid line; heat capacity anomaly effect), and residual (dark-gray dot-dash line) are shown. MLD anomalies (light-blue solid line) are superimposed (in m; right y axis label). Filled (open) markers show anomalies exceeding the 90% (80%) confidence level in a two-tailed  $t$  test. A 3 month running mean is applied to smooth the time series. (b, d) As in Figures 7a and 7c, but for the nonlocally amplified case.

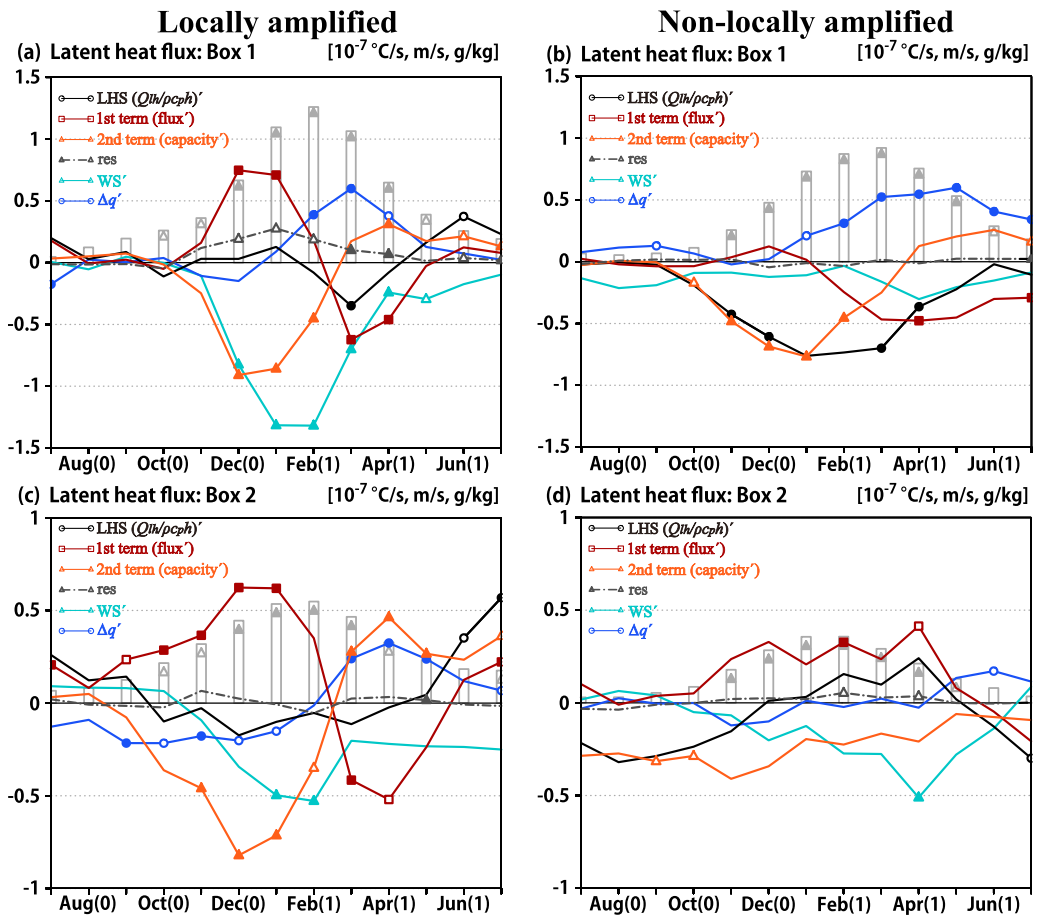


**Figure 8.** Time series of composite anomalies of the latent heat terms in equation (7) over the Box 1 region for (a) the locally amplified and (b) the nonlocally amplified Ningaloo Niño (in  $10^{-7}^{\circ}\text{C/s}$ ). (c, d) As in Figures 7a and 7b, respectively, but for the Box 2 region with a different vertical scale from Figures 7a and 7b. The total contribution anomaly (black solid line), the first term (dark-red solid line; flux anomaly effect), the second term (orange solid line; heat capacity anomaly effect), and residual (dark-gray dot-dash line) are shown. Wind speed (in m/s; WS; light-blue solid line), the difference between the saturated specific humidity at SST and the specific humidity at 2 m (in g/kg;  $\Delta q$ ; blue solid line), and SST (in  $^{\circ}\text{C}$ ; light gray bar) anomalies are superimposed. Filled (open) markers show anomalies exceeding the 90% (80%) confidence level in a two-tailed  $t$  test. A 3 month running mean is applied to smooth the time series.

capacity variation effect (Figure 8a): While *anomalous* latent heat flux consistent with previous studies is seen during the peak phase (the first term on the RHS of equation (7) with  $Q'_{LH} > 0$ ), it is canceled out by the enhanced *climatological* cooling due to the anomalously thin mixed-layer (the second term on the RHS of equation (7) with  $\bar{Q}_{LH} < 0$  and  $h' < 0$ ). Neglecting this second term effect led the previous studies to conclude that the latent heat flux directly forces SST anomalies. The time evolution of the latent heat flux anomaly is closely related to the reduction in wind speed (Figure 8a), and this reduction in the wind speed also contributes to the shoaling of the MLD.

The decay of warm anomalies in early autumn is explained by the sum of the anomalous contribution from the shortwave radiation, and latent and sensible heat fluxes, while the relative importance of the meridional advection anomaly becomes larger after April (1). This meridional advection anomaly is associated with the weakening of the meridional temperature gradient (interannually smaller  $|\nabla T'|$ ) and the seasonally intensified Leeuwin Current (seasonally larger  $|\bar{v}'|$ ), the former being likely due to the preceding anomalous current (Figure 6a). The anomalous contribution from the shortwave radiation in this phase is associated with the suppressed climatological warming owing to thickening of MLD (Figure 7a). On the other hand, the anomalous cooling by the sensible heat flux associated with flux anomaly (figure not shown), which is expected from higher SSTs, contributes to the decay. Similarly, anomalous cooling by the latent heat flux is associated with the increased evaporation (Figure 8a). Since positive SST anomalies grow while reduced wind speed

recovers, the increase in surface evaporation associated with that in SST eventually overwhelms the decrease in surface evaporation associated with that in wind speed and contributes to the damping of SST anomalies. This is reflected in the increase of anomalous specific humidity difference  $\Delta q$ .

#### 5.1.1.2. Offshore Region

Over the offshore region (i.e., Box 2), the MLT tendency is mostly controlled by the contribution from the shortwave radiation during the whole life cycle (Figure 5c), where MLD anomalies again play an important role (Figure 7c). The vertical processes damp SST anomalies owing to their more efficient cooling of the thinner mixed-layer. Also, a significant positive  $\Delta T$  anomaly in February (1) contributes to the cooling by the vertical processes.

Again, we note that no significant contribution from the latent heat flux is found, contrary to previous studies suggesting that latent heat flux anomalies generate SST anomalies (e.g., Kataoka et al., 2014; Marshall et al., 2015). Similar to the coastal region, positive latent heat flux anomalies (Figure 8c) are seen with a reduction in the wind speed, but they are compensated by enhanced climatological cooling owing to shallower mixed-layer. In other words, the positive first term on the RHS of equation (7) with  $Q'_{LH} > 0$  is offset by the negative second term with  $\overline{Q_{LH}} < 0$  and  $h' < 0$ . Therefore, the positive latent heat flux anomalies do not directly warm the mixed-layer. However, this does not mean that the latent heat flux is unimportant; through buoyancy flux, its anomalies can cause MLD variation, which plays a key role in generating SST anomalies as discussed above. In fact, latent heat flux anomalies dominate surface heat flux anomalies (figure not shown) and some coherency is seen between the heat flux anomaly term of the latent heat (Figure 8c) and MLD anomalies (Figure 7c), while negative wind speed anomalies themselves may also contribute to anomalously shallow mixed-layer.

In the decay season, the SST response becomes important in latent heat flux anomalies and they change the sign, but the capacity variation effect again compensates this term. Thus, the variation in the latent heat flux itself does not directly contribute to the evolution of the MLT anomaly.

#### 5.1.2. Nonlocally Amplified Case

##### 5.1.2.1. Coastal Region

Now let us consider the nonlocally amplified case. Anomalies in the meridional advection and the contribution from the shortwave radiation cause anomalous warming of the mixed-layer. It is found that the anomalously strong current (Figure 6b; the third term on the RHS of equation (11) with  $\mathbf{v}' < 0$ ) and the smaller mixed-layer heat capacity (Figure 7b; the third term on the RHS of equation (10) with  $\overline{Q_{SW}} > 0$  and  $h' < 0$ ) are again responsible for those anomalies. The anomalously strong Leeuwin Current is mainly driven by the ENSO through coastal waves (e.g., Feng et al., 2013; Kataoka et al., 2014; Marshall et al., 2015). As noted in the introduction, the remote forcing on the Leeuwin Current is seen in some of the locally amplified Ningaloo Niño events, in which the current is further accelerated by local wind anomalies and thus, the current anomalies are larger than nonlocally amplified events (Figures 6a and 6b). In addition to the stronger current, the seasonally intensified meridional temperature gradient (Figure 3; seasonally larger  $|\nabla T|$ ) offers a favorable condition for the anomalous meridional advection related to the third term on the RHS of equation (11). Although the MLD is anomalously shallow, neither significant wind speed (Figure 8b) nor net surface heat flux anomalies (figure not shown) are found during the developing season. The anomalous poleward current may contribute to the shallower MLD by advecting the warm and fresh water from the tropics (e.g., Feng et al., 2015), although its details are left for future study. These negative MLD anomalies may result in the stronger than normal cooling by the vertical processes during summer. In contrast to the locally amplified case, the latent heat flux contributes to damping of MLT anomalies. This difference is mostly explained by the difference in the flux anomaly (Figures 8a and 8b). As expected from Figure 4a, we cannot see wind speed reduction and latent heat flux anomalies for the nonlocally amplified case (Figure 8b). Thus, the enhanced climatological cooling is not canceled out as in the locally amplified case.

From late summer to autumn, positive SST anomalies lead to larger latent heat release and the negative feedback by anomalous latent heat flux takes over the enhanced climatological latent heat loss associated with the thinner mixed-layer. Negative meridional advection anomalies contribute to the cooling at the final decay stage. This seems to be due to the combination of the weaker meridional temperature gradient and the current, though the former is not statistically significant. We note that the stronger climatological current in this season also contributes to the negative meridional advection anomaly associated with the fourth term on the RHS of equation (11).

5.1.2.2. Offshore Region

For the offshore region, almost no statistically significant anomalies are found and we cannot discuss in detail (Figure 5d). However, we note the importance of the enhanced warming by the climatological short-wave radiation as for the locally amplified case (Figure 7d).

5.2. Ningaloo Niña

Since only three Ningaloo Niña events are classified into the locally amplified case during 1958–2012 (Figure 4b), we first discuss the nonlocally amplified case and then briefly comment on the locally amplified case.

5.2.1. Nonlocally Amplified Case

5.2.1.1. Coastal Region

From spring to summer, the anomalous MLT cooling is mainly caused by an anomalous meridional advection (Figure 9b), which is associated with the weakening of the Leeuwin Current (Figure 10b; the third term of equation (11) with  $v' > 0$ ). The seasonally intensified meridional temperature gradient in summer (Figure 3; seasonally larger  $|\nabla T|$  in the third term on the RHS of equation (11)) also contributes to the development of the anomaly in this term. As in the nonlocally amplified Ningaloo Niña case, the anomalous contribution from the latent heat flux damps the MLT anomalies around summer. This is explained by positive latent heat flux anomalies (Figure 11b; the first term on the RHS of equation (7) with  $Q'_{LH} > 0$ ), associated with the cooler SST and smaller  $\Delta q$  (Figure 11b).

At the early stage of the decay phase, the anomalous contribution from the sensible heat flux plays a role in warming. We find that this anomalous contribution is related to positive sensible heat flux anomalies due to negative MLT anomalies, though they are not significant until April (1) (figure not shown). As SST anomalies decay, the anomalous latent heat flux also becomes smaller. At the same time, the MLD becomes thinner (Figure 12b), which is related to positive net surface heat flux anomalies (figure not shown), resulting in

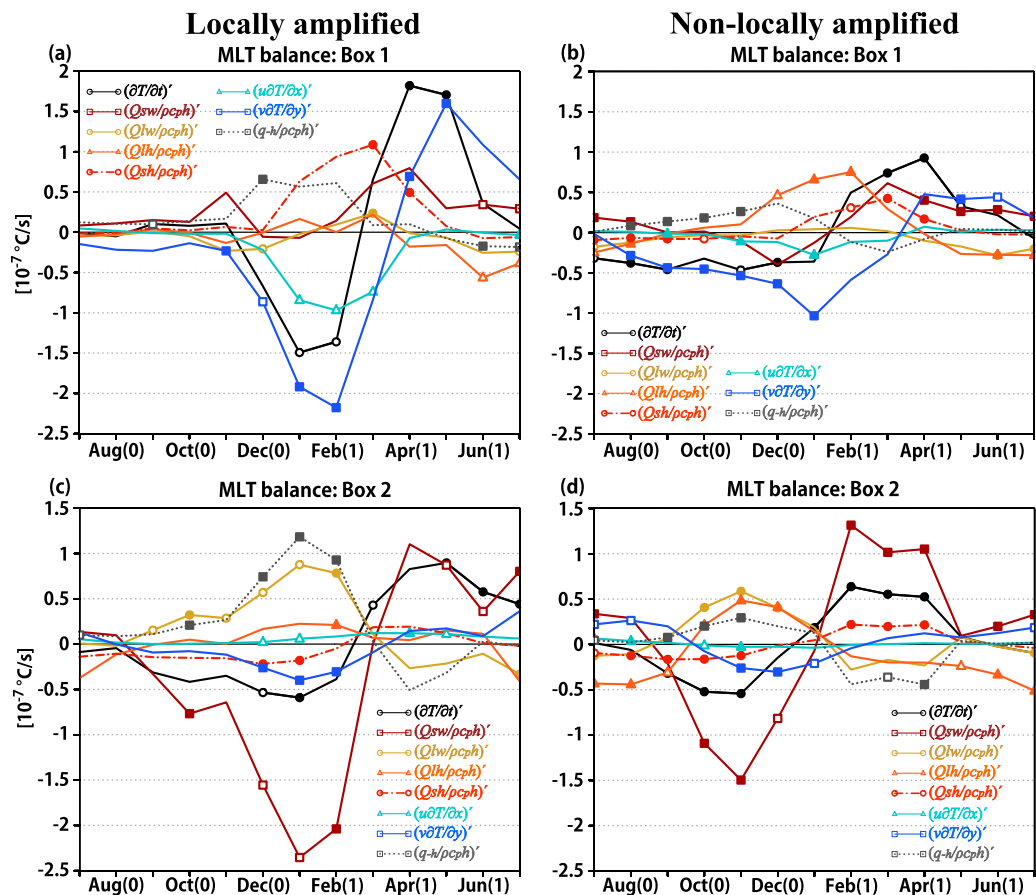


Figure 9. As in Figure 5, but for Ningaloo Niña. Note that only three Ningaloo Niña events are classified as the locally amplified case.

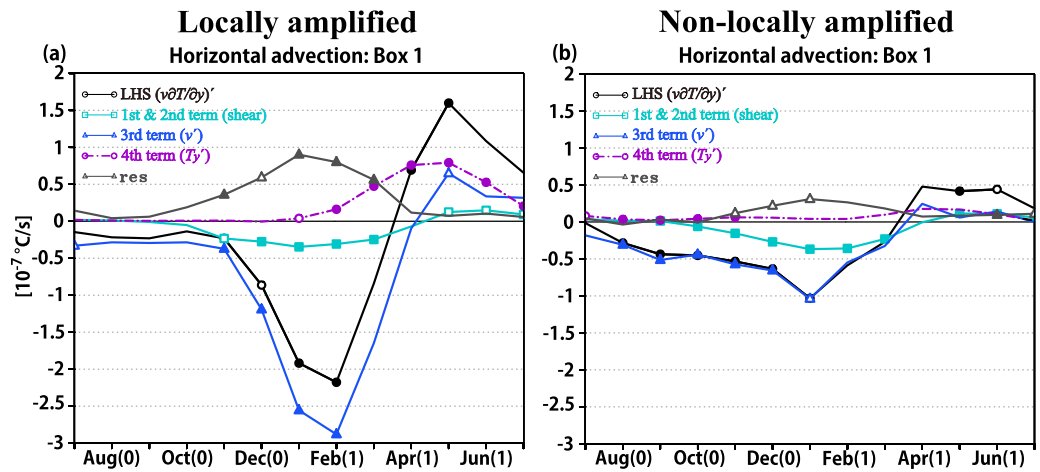


Figure 10. As in Figure 6, but for Ningaloo Niña.

enhanced cooling by the climatological latent heat flux (Figure 11b; the second term on the RHS of equation (7) with  $\overline{Q_{LH}} < 0$  and  $h' < 0$ ). The latter overwhelms the former by April (1) and the anomalous contribution from the latent heat flux moderates the decay of the MLT anomalies at the very final stage. The

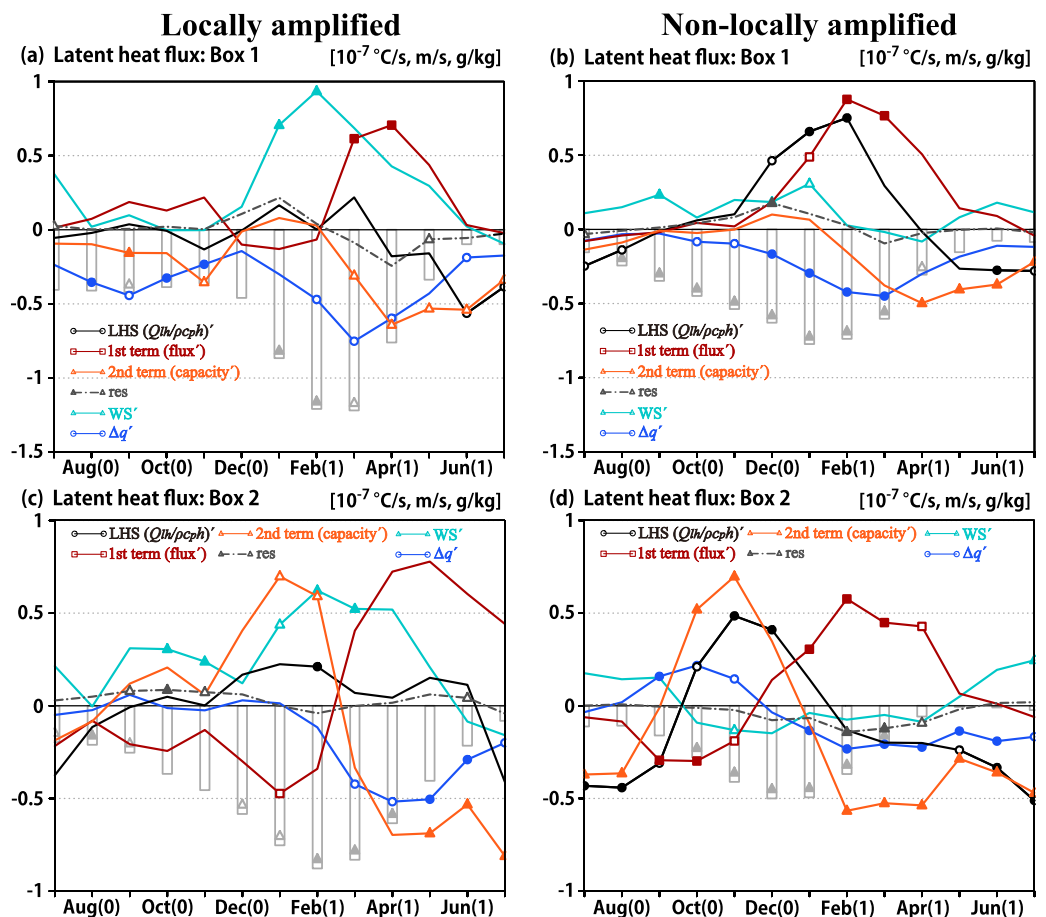


Figure 11. As in Figure 8, but for Ningaloo Niña.

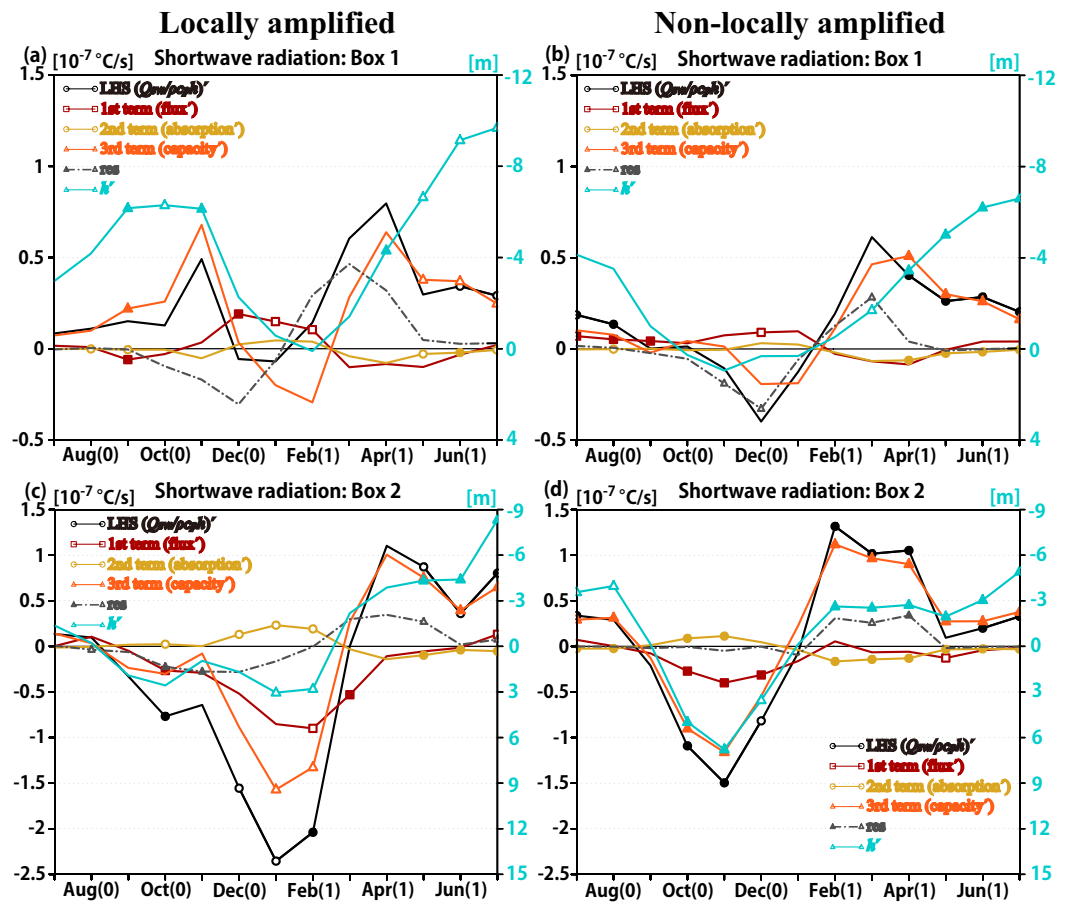
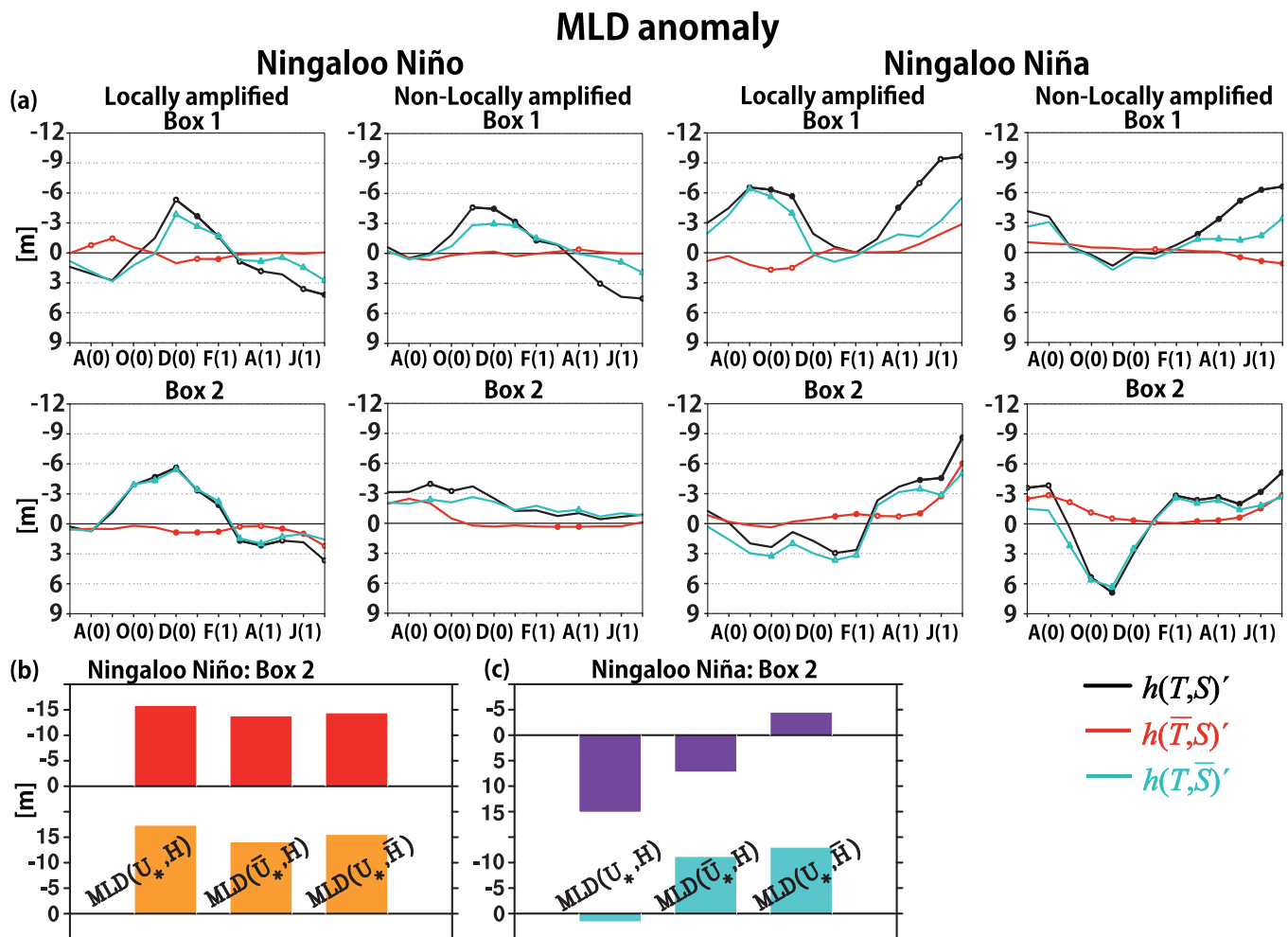


Figure 12. As in Figure 7, but for Ningaloo Niña. Different vertical scales are used between the two regions.

anomalous contribution from the shortwave radiation also contributes to the decay and is associated with the enhanced warming by the shallower MLD (Figure 13b; the third term on the RHS of equation (10) with  $\overline{Q_{sw}} > 0$  and  $h' < 0$ ). At last, meridional advection anomalies seem to warm the MLT, although SST anomalies are no longer significant then.

5.2.1.2. Offshore Region

Figure 9d shows the MLT balance anomaly for the offshore region. For both the growth and decay periods, the MLT tendency anomaly in Box 2 is primarily controlled by the anomalous contribution from the shortwave radiation, which is explained by the heat capacity variation, highlighting the importance of MLD anomalies again (Figure 12d). Around the peak phase, the anomalous contribution from the longwave radiation tends to oppose the MLT cooling due to the combination of its suppressed climatological cooling owing to thicker mixed-layer (the second term on the RHS of equation (7) with  $\overline{Q_{LW}} < 0$  and  $h' > 0$ ) and downward longwave radiation anomaly (the first term on the RHS of equation (7) with  $Q'_{LW} > 0$ ). The anomalous contribution from the latent heat flux also damps the MLT cooling. This is different from the inference made by Kataoka et al. (2014) based on the spatial pattern (therefore, assuming a constant MLD). This apparent discrepancy again can be understood by the decomposition of equation (7) (Figure 11d); latent heat flux anomalies themselves are negative (the first term on the RHS of equation (7) with  $Q_{LH}' < 0$ ), but the diluted climatological cooling associated with the deeper MLD (the second term on the RHS of equation (7) with  $\overline{Q_{LH}} < 0$  and  $h' > 0$ ) overwhelms, resulting in damping of negative SST anomalies. This damping effect of the latent heat flux is contrasted from that for the nonlocally amplified Ningaloo Niña, where no significant role of the latent heat flux is seen (Figure 5a). The difference seems to be related to smaller latent heat flux anomalies due to smaller wind speed anomalies during the developing phase of the nonlocally amplified Ningaloo Niña.



**Figure 13.** (a) Composites of MLD anomalies computed using interannually varying temperature and salinity (black), monthly climatology of temperature and interannually varying salinity (red), and interannually varying temperature and monthly climatology of salinity (light blue) during Ningaloo Niño/Niña years. Filled (open) markers show anomalies exceeding the 90% (80%) confidence level in a two-tailed *t* test. A 3 month running mean is applied to smooth the time series. (b) Composite of MLD anomalies diagnosed by equation (12) in DJF for (top) locally amplified and (bottom) nonlocally amplified Ningaloo Niño over the Box 2 region (in m). Middle (right) bars show diagnosed values with the monthly climatology of frictional velocity (surface heat flux). Note that 1998/1999 and 1999/2000 events are excluded from the nonlocally amplified Ningaloo Niño composites. (c) As in Figure 13b), but for Ningaloo Niña.

### 5.2.2. Locally Amplified Case

Although only three Ningaloo Niña events are classified into the locally amplified case, they are similar to the nonlocally amplified case; anomalous meridional advection due to the weaker Leeuwin Current is important for the coastal region, whereas the reduced warming by the shortwave radiation owing to the deeper MLD dominates the anomalous cooling in the offshore region. The damping effect of the latent heat flux is seen as in the nonlocally amplified Ningaloo Niña and is different from the locally amplified Ningaloo Niño, which may stem from a smaller wind speed anomaly and resulting smaller latent heat flux anomaly. If Ningaloo Niña events with a negative CWI are classified as the locally amplified case, we have 8 locally amplified Ningaloo Niña events. Under this criterion, shortwave radiation anomalies themselves as well as reduced warming by the climatological shortwave radiation owing to thicker mixed-layer contributes to the offshore SSTA development.

### 5.3. Interannual Anomalies of MLD Related to Ningaloo Niño/Niña

As discussed in the previous two subsections, MLD anomalies are important for the life cycle of Ningaloo Niño/Niña in the offshore region and that of Ningaloo Niño in the coastal region. To investigate this further, the MLD is diagnosed again using the monthly climatology for either temperature or salinity:  $h(\bar{T}, S)$  and  $h(T, \bar{S})$ , respectively. It is revealed that MLD variability related to Ningaloo Niño/Niña is mostly determined

by vertical variations of temperature rather than salinity variations since  $h(T, \bar{S})'$  better reproduces  $h'$  (Figure 13a). Interestingly, salinity variations also contribute to MLD anomalies from August (0) to November (0) during the strongest Ningaloo Niño in 2010/2011. However, we should note that our model does not have the freshwater flux as the surface boundary condition and SSSs are restored to the observed monthly mean climatology, which may underestimate the salinity control of MLD. In fact, freshening anomalies are observed until June 2011 during the strongest Ningaloo Niño event (Feng et al., 2015).

For a further discussion on the cause of MLD anomalies, a diagnostic value of MLD under the stabilizing surface flux is calculated based on the following equation (Zilitinkevich et al., 2002):

$$\text{MLD}(U^*, H) = \frac{\kappa U^*}{|f|(a+bZ)^{1/2}}. \quad (12)$$

Here  $U^*$  is the frictional velocity,  $H$  surface heat flux,  $\kappa=0.4$  the von Kármán constant, “stabilizing flux”  $Z = -B/|f|U^{*2}$ , buoyancy flux  $B = -g[\alpha H/c_p \rho - \beta(E-P)S]$ ,  $g$  the gravity acceleration,  $\alpha$  the thermal expansion coefficient,  $\beta$  the haline contraction coefficient,  $E-P$  the surface freshwater flux, and SSS is used for mixed-layer salinity  $S$ , and 0.28 and 0.31 are adopted for empirical constants  $a$  and  $b$ , respectively (Yoshikawa, 2015). Since the horizontal advection is assumed to be weak in this formulation, only the MLD over Box 2 is diagnosed. The monthly climatology of diagnosed MLD during summer is generally deeper than the observed or simulated MLD climatology (Figure 2b). Nevertheless, it reproduces deeper MLDs in December, which tend to shallow into February (91 m in December, 54 m in January, and 39 m in February), and may give a qualitative insight into generation of MLD anomalies during summer.

A composite of diagnosed MLD anomaly shows a negative value during the Ningaloo Niño years consistent with our simulation, though the amplitude is larger (Figure 13b). The shallower mixed-layer is explained by a combination of the stronger buoyancy gain and weaker wind stirring because we obtain a deeper MLD if we use a climatological value either for the frictional velocity or surface heat flux. Although the monthly climatology of SSSs is used to focus on the relative importance of surface heat flux and wind stirring, the results are unchanged within 5% even if interannually varying SSSs are imposed. Note that, for the nonlocally amplified case, 1998/1999 and 1999/2000 events are excluded from the composites because equation (12) gives unrealistically deep MLD anomalies in December for those events (the MLD anomalies are 73 and 241 m, respectively).

When equation (12) is applied to Ningaloo Niña events, the MLD anomalies during the locally amplified case are mainly explained by the surface heat flux, while the subdominant contribution from the winds are also seen (Figure 13c, top). MLD anomalies during nonlocally amplified case are related to both surface heat flux and wind speed anomalies (Figure 13c, bottom). However, we note again that only three Ningaloo Niña events are classified into the locally amplified case.

## 6. Discussions

This study revealed the importance of MLD anomalies, which change sensitivity of the mixed-layer to the surface heat fluxes. Among others, the sensitivity change to the climatological shortwave radiation offers a

following possible feedback process. Positive SST anomalies generate low-pressure anomalies in the overlying atmosphere. Since the accompanied wind anomalies are against the climatological winds, the mixed-layer becomes anomalously shallow because of weaker wind stirring and/or reduced latent heat loss, resulting in an enhanced warming by the climatological shortwave radiation. Because the ocean model used in this study does not incorporate atmospheric feedback, the above feedback should be explored using a coupled model.

We note that the change in sensitivity is not directly proportional to MLD anomalies but proportional to their ratio to the climatology, as inferred from equations (7) and (10). Figure 14 shows the standard deviation of MLD anomalies over the NNI region along with their ratio to the climatology. Although the standard deviation is relatively small

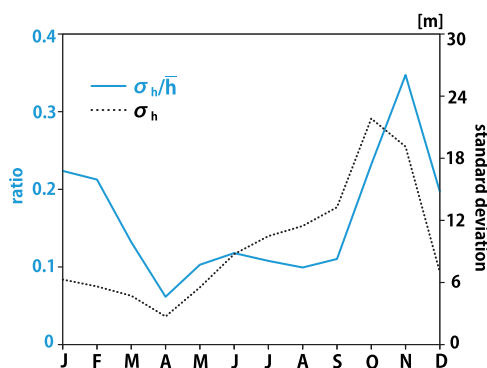


**Figure 14.** Monthly standard deviation of the MLD over the NNI region (in m; black dotted line) and its ratio to the climatology (blue solid line).

during summer, the ratio is large from spring to summer, when Ningaloo Niño/Niña develops (Figure 1c). This suggests that the seasonal phase-locking nature is related to the seasonal variation of the MLD.

We further note that the sign as well as the amplitude of the climatological surface heat fluxes could also contribute to the phase-locking nature. Northerly (southerly) alongshore wind anomalies, for example, may generate positive (negative) SST anomalies via strengthened (weakened) meridional advection. Given the climatological southerly, these northerly (southerly) wind anomalies lead to a shallower (deeper) mixed-layer. If the climatological net surface heat flux tends to warm the mixed-layer, the smaller (larger) heat capacity enhances the warming (cooling) tendency anomalies. However, if the climatological net surface heat flux cools the mixed-layer, it reduces, or even offsets the warming (cooling) by the advection. As seen in Figure 2, summer is the only season when the net surface heat flux warms the mixed-layer.

Such an effect of interannual MLD variation is also crucial for development of other climate modes such as the Atlantic Meridional Mode (Doi et al., 2010) and the Subtropical Dipole Modes (Morioka et al., 2010; Kataoka et al., 2012). The above discussion on the seasonal phase-locking nature may be applicable to these climate modes (e.g., Suzuki et al., 2004) and may even be extended to their changes on longer timescales (e.g., Yamagami & Tozuka, 2015).

## 7. Conclusions

Using outputs from an OGCM, we have quantitatively examined the generation and decay mechanisms of SST anomalies associated with Ningaloo Niño/Niña taking MLD variations into account. Since Ningaloo Niño/Niña is suggested to develop as the result of a combination of local air-sea coupling and remote forcing (Kataoka et al., 2014; Marshall et al., 2015), events are classified into two cases and analyzed separately. Also, MLT balance is calculated for the coastal and offshore regions because each region may be governed by different processes.

For the coastal region, positive meridional advection anomalies associated with the stronger Leeuwin Current (the third term on the RHS of equation (11) with  $\mathbf{v}' < 0$ ) and enhanced warming by climatological shortwave radiation owing to anomalously thin mixed-layer (the third term on the RHS of equation (10) with  $\overline{Q_{SW}} > 0$  and  $h' < 0$ ) contribute to the generation of both cases of Ningaloo Niño. The former supports the existence of the local positive feedback proposed by Kataoka et al. (2014). Seasonal intensification of meridional temperature gradient in summer (a larger  $|\nabla\bar{T}|$  in the third term on the RHS of equation (11)) is favorable for a larger advection anomaly and thus, for the seasonal development of the phenomenon. On the other hand, negative sensible heat flux anomalies play an important role in the decay. Since the positive meridional advection anomalies during the developing phase reduce the meridional temperature gradient, meridional advection anomalies eventually change their sign and also contribute to the decay (the fourth term on the RHS of equation (11) with  $\nabla T' < 0$ ). Seasonally strong Leeuwin Current (seasonally larger  $|\bar{\mathbf{v}}|$  in the fourth term on the RHS of equation (11)) contributes to a larger anomaly as well and therefore, to the decay of Ningaloo Niño from autumn to winter.

However, there are some differences between the two cases. For the locally amplified case, anomalous northerly alongshore winds oppose climatological southerly winds, and the resulting weaker wind speed leads to smaller latent heat loss (the first term on the RHS of equation (7) with  $Q'_{LH} > 0$ ; the flux anomaly effect). This is mostly cancelled out by enhanced cooling by climatological latent heat loss associated with the shallower mixed-layer (the second term on the RHS of equation (7) is negative with  $\overline{Q_{LH}} < 0$  and  $h' < 0$ ; the capacity variation effect). This is why the latent heat flux as a whole does not contribute much to the development. However, this does not mean that the latent heat flux is unimportant; through buoyancy flux, its anomalies can cause MLD variation, which plays a key role in generating SST anomalies as discussed above. For the nonlocally amplified case, on the other hand, no significant wind speed anomalies are seen and thus no significant latent heat flux anomalies are found during the developing season (the first term on the RHS of equation (7) with  $Q_{LH}' \approx 0$ ). However, enhanced cooling by climatological latent heat loss is present (the second term on the RHS of equation (7) is negative with  $\overline{Q_{LH}} < 0$  and  $h' < 0$ ). While this enhancement weakens after the peak phase, negative latent heat flux anomalies become larger owing to warm SST anomalies. As a result, the latent heat flux as a whole cools the mixed-layer throughout the course of the event. Neglecting interannual MLD variations ( $h'$ ) led the previous studies to the conclusion that the latent

heat flux directly contributes to SST anomalies (e.g., Feng et al., 2013; Kataoka et al., 2014; Marshall et al., 2015).

The MLT tendency anomalies in the offshore region during the development (decay) phase for both cases are dominated by enhanced (reduced) warming by the climatological shortwave radiation owing to negative (positive) MLD anomalies, which is controlled by vertical variations in temperature rather than salinity. An MLD diagnosis suggests that anomalies in both surface heat flux and wind stress are important for MLD anomalies. While past studies (e.g., Feng et al., 2013; Kataoka et al., 2014; Marshall et al., 2015) argued that latent heat flux anomalies contribute to the warming, no significant contribution from the latent heat flux is seen in this study. The difference again can be understood by a balance between the flux anomaly effect and the capacity variation effect, where the latter was not taken into account in the previous studies based on the assumption that  $h' = 0$ .

The generation and decay mechanisms for both cases of Ningaloo Niña are close to a mirror image of those for Ningaloo Niño in general. In particular, negative meridional advection anomalies associated with the weaker Leeuwin Current and suppressed warming by climatological shortwave radiation play an important role in the coastal and offshore regions, respectively, in the development. However, there is a difference as well. In the offshore region, the latent heat flux tends to dampen MLT anomalies during the developing season for both cases of Ningaloo Niña, whereas no significant contribution from the latent heat flux as a whole is seen during both cases of Ningaloo Niño. However, we note that only three locally amplified cases occurred and we need more events to discuss their general characteristics.

#### Acknowledgments

We thank Harry Hendon for helpful discussions and for providing PEODAS data and Chiarui Ong for a helpful discussion on the supporting information. Constructive comments from two anonymous reviewers were helpful in improving the manuscript. ERSST and NCEP/NCAR reanalysis data were provided by the NOAA/OAR/ESRL PSD, Boulder, CO, from their web site at <http://www.esrl.noaa.gov/psd/>; PEODAS Re-Analysis at [http://poama.bom.gov.au/data\\_server.shtml](http://poama.bom.gov.au/data_server.shtml); CARS2009 at <http://www.marine.csiro.au/~dunn/cars2009/>; and the sea level at Fremantle at <http://www.bom.gov.au/oceanography/projects/ntc/ntc.shtml>. The present research was supported by the Japan Society for Promotion of Science through Grant-in-Aid for Scientific Research (B) JP16H04047. T.K. was supported by Research Fellowship of the Japan Society for the Promotion of Science (JSPS) for Young Scientists, by Leading Graduate Course for Frontiers of Mathematical Sciences and Physics, and by the Sasakawa Scientific Research Grant from the Japan Science Society. T.Y. was supported by the Environment Research and Technology Development Fund (2-1405) of the Ministry of the Environment, Japan.

#### References

- Benthuisen, J., Feng, M., & Zhong, L. (2014). Spatial patterns of warming off Western Australia during the 2011 Ningaloo Niño: Quantifying impacts of remote and local forcing. *Continental Shelf Research*, *91*, 232–246.
- Carton, J. A., & Giese, S. G. (2008). A reanalysis of ocean climate using Simple Ocean Data Assimilation (SODA). *Monthly Weather Review*, *136*, 2999–3017.
- Clarke, A. J. (1991). On the reflection and transmission of low-frequency energy at the irregular western Pacific Ocean boundary. *Journal of Geophysical Research*, *96*, 3289–3305.
- Clarke, A. J., & Liu, X. (1994). Interannual sea level in the northern and eastern Indian Ocean. *Journal of Physical Oceanography*, *24*, 1224–1235.
- Dee, D. P., Uppala, S. M., Simmons, A. J., Berrisford, P., Poli, P., Kobayashi, S., . . . Vitart, F. (2011). The ERA-Interim reanalysis: configuration and performance of the data assimilation system. *Quarterly Journal of the Royal Meteorological Society*, *137*, 553–597.
- Doi, T., Tozuka, T., & Yamagata, T. (2010). The Atlantic Meridional Mode and its coupled variability with the Guinea Dome. *Journal of Climate*, *23*, 455–475.
- Feng, M., Benthuisen, J., Zhang, N., & Slawinski, D. (2015). Freshening anomalies in the Indonesian throughflow and impacts on the Leeuwin Current during 2010–2011. *Geophysical Research Letters*, *42*, 8555–8562. <https://doi.org/10.1002/2015GL065848>
- Feng, M., McPhaden, M. J., Xie, S.-P., & Hafner, J. (2013). La Niña forces unprecedented Leeuwin Current warming in 2011. *Scientific Reports*, *3*, 1277. <https://doi.org/10.1038/srep01277>
- Feng, M., Meyers, G., Pearce, A., & Wijffels, S. (2003). Annual and interannual variations of the Leeuwin Current at 32°S. *Journal of Geophysical Research*, *108*(C11), 3355. <https://doi.org/10.1029/2002JC001763>
- Godfrey, J. S., & Ridgway, K. R. (1985). The large-scale environment of the poleward-flowing Leeuwin Current, Western Australia: Longshore steric height gradients, wind stresses and geostrophic flow. *Journal of Physical Oceanography*, *15*, 481–495.
- Ide, Y., & Yoshikawa, Y. (2016). Effects of diurnal cycle of surface heat flux on wind-driven flow. *Journal of Oceanography*, *72*, 263–280.
- Jerlov, N. G. (1976). *Marine optics* (231 pp.). Amsterdam, the Netherlands: Elsevier.
- Kalnay, E., Kanamitsu, M., Kistler, R., Collins, W., Deaven, D., Gandin, L., . . . Joseph, D. (1996). The NCEP/NCAR 40-year reanalysis project. *Bulletin of the American Meteorological Society*, *77*, 437–471.
- Kataoka, T., Tozuka, T., Behera, S., & Yamagata, T. (2014). On the Ningaloo Niño/Niña. *Climate Dynamics*, *43*, 1463–1482.
- Kataoka, T., Tozuka, T., Masumoto, Y., & Yamagata, T. (2012). The Indian Ocean subtropical dipole mode simulated in the CMIP3 models. *Climate Dynamics*, *39*, 1385–1399.
- Kido, S., Kataoka, T., & Tozuka, T. (2016). Ningaloo Niño simulated in the CMIP5 models. *Climate Dynamics*, *47*, 1469–1484.
- Levitus, S., & Boyer, T. P. (1994). World ocean atlas, vol. 4: Temperature. In *NOAA atlas NESDIS 4* (117 pp.). Washington, DC: U.S. Government Printing Office.
- Levitus, S., Burgett, R., & Boyer, T. P. (1994). World ocean atlas, vol. 3: Salinity. In *NOAA atlas NESDIS 3* (99 pp.). Washington, DC: U.S. Government Printing Office.
- Marshall, A. G., Hendon, H. H., Feng, M., & Schiller, A. (2015). Initiation and amplification of the Ningaloo Niño. *Climate Dynamics*, *45*, 2367–2385.
- Meyers, G. (1996). Variation of the Indonesian throughflow and the El Niño Southern Oscillation. *Journal of Geophysical Research*, *101*, 12255–12263.
- Morioka, Y., Tozuka, T., & Yamagata, T. (2010). Climate variability in the southern Indian Ocean as revealed by self-organizing maps. *Climate Dynamics*, *35*, 1059–1072.
- Pacanowski, R. C., & Griffies, S. M. (1999). *MOM 3.0 manual*. Princeton, NJ: NOAA/GFDL.
- Pacanowski, R. C., & Philander, S. G. H. (1981). Parameterization of vertical mixing in numerical models of tropical oceans. *Journal of Physical Oceanography*, *11*, 1443–1451.
- Paulson, C. A., & Simpson, J. J. (1977). Irradiance measurements in the upper ocean. *Journal of Physical Oceanography*, *7*, 952–956.
- Pearce, A. F., & Feng, M. (2013). The rise and fall of the “marine heat wave” off Western Australia during the summer of 2010/2011. *Journal of Marine Systems*, *111–112*, 139–156.

- Ridgway, K. R., Dunn, J. R., & Wilkin, J. L. (2002). Ocean interpolation by four-dimensional weighted least squares—Application to the waters around Australia. *Journal of Atmospheric and Oceanic Technology*, *19*, 1357–1375.
- Smagorinsky, J. (1963). General circulation experiments with the primitive equations. Part I: The basic experiment. *Monthly Weather Review*, *91*, 99–164.
- Smith, R. L., Huyer, A., Godfrey, J. S., & Church, J. A. (1991). The Leeuwin Current off Western Australia, 1986–1987. *Journal of Physical Oceanography*, *21*, 323–345.
- Smith, T. M., Reynolds, R. W., Peterson, T. C., & Lawrimore, J. (2008). Improvements to NOAA's historical merged land-ocean surface temperature analysis (1880–2006). *Journal of Climate*, *21*, 2283–2296.
- Suzuki, R., Behera, S. K., Iizuka, S., & Yamagata, T. (2004). Indian Ocean subtropical dipole simulated using a couple general circulation model. *Journal of Geophysical Research*, *109*, C09001. <https://doi.org/10.1029/2003JC001974>
- Tozuka, T., Kataoka, T., & Yamagata, T. (2014). Locally and remotely forced atmospheric circulation anomalies of Ningaloo Niño/Niña. *Climate Dynamics*, *43*, 2197–2205.
- Vialard, J., & Delecluse, P. (1998). An OGCM study for the TOGA decade. Part I: Role of salinity in the physics of the western Pacific fresh pool. *Journal of Physical Oceanography*, *28*, 1071–1088.
- Wernberg, T., Smale, D. A., Tuya, F., Thomsen, M. S., Langlois, T. J., de Bettignies, T., . . . Rousseaux, C. S. (2012). An extreme climatic event alters marine ecosystem structure in a global biodiversity hotspot. *Nature Climate Change*, *3*, 78–82.
- Yamagami, Y., & Tozuka, T. (2015). Interdecadal changes of the Indian Ocean subtropical dipole mode. *Climate Dynamics*, *44*, 247–258.
- Yin, Y., Alves, O., & Oke, P. R. (2011). An ensemble ocean data assimilation system for seasonal prediction. *Monthly Weather Review*, *139*, 786–808.
- Yoshikawa, Y. (2015). Scaling surface mixing/mixed layer depth under stabilizing buoyancy flux. *Journal of Physical Oceanography*, *45*, 247–258.
- Zilitinkevich, S., Baklanov, A., Rost, J., Smedman, A.-S., Lykosov, V., & Calanca, P. (2002). Diagnostic and prognostic equations for the depth of the stably stratified Ekman boundary layer. *Quarterly Journal of the Royal Meteorological Society*, *128*, 25–46.